Cover illustration

Special issue:
Nanobio vs. bionano
As researchers develop capabilities to engineer and manipulate objects and systems at ever-diminishing scales, we are now entering the realm of scientific discoveries at the nano-level. One such invention is pictured on the cover of this Special Issue, edited by François Baneyx (University of Washington, USA) and Je-Kyun Park (KAIST, Korea), showing a single-cell-sized neural electrode with unique gold nanograin structures in the beautiful shape of a sunflower. Image: © Yoonkey Nam

Biotechnology Journal – list of articles published in the February 2013 issue.

DOI 10.1002/biot.201200219 Biotechnol. J. 2013, 8, 206–214

Research Article

Gold nanograin microelectrodes for neuroelectronic interfaces

Raeyoung Kim, Nari Hong and Yoonkey Nam

Department of Bio and Brain Engineering, KAIST, Daejeon, Korea

Neuroelectronic interfaces are imperative in investigating neural tissues as electrical signals are the main information carriers in the nervous system and metal microelectrodes have been widely used for recording and stimulation of nerve cells. For high performance microelectrodes, low tissue-electrode interfacial impedance and high charge injection limits are essential and nanoscale surface engineering has been utilized to meet the requirements for microelectrodes. We report a single-cell sized microelectrode, which has unique gold nanograin structures, using a simple electrochemical deposition method. The fabricated microelectrode had a sunflower shape with 1–5 μm of micropetals along the circumference of the microelectrode and 500 nm nanograins at the center. The nanograin electrodes had 69-fold decrease of impedance and 10-fold increase in electrical stimulation capability compared to unmodified flat gold microelectrodes. The recording and stimulation performance of nanograin electrodes was tested using dissociated rat hippocampal neuronal cultures. Noise levels were extremely low (2.89 μV_{rms}) resulting in high signal-to-noise ratio for low-amplitude action potentials (18.6–315 μV). Small biphasic current pulses (20–60 μA) could evoke action potentials from neurons nearby electrodes. This new nanostructured neural electrode may be applicable for the development of cell-based biosensors or clinical neural prosthetic devices.

Received	30 MAY 2012
Revised	14 SEP 2012
Accepted	10 OCT 2012
Accepted article online	16 OCT 2012

Supporting information available online

Keywords: Electrical stimulation · Gold nanostructure · Microelectrode · Neural interface · Neural recording

1 Introduction

Electrophysiological nature of neural networks has long been studied to understand the fundamentals of brain functions. A series of electrical pulses, called action potentials, are generated by individual neurons and they carry salient information in neural networks. Neuroelectronic interfaces are the connection point between neurons and electronic systems and microelectrodes have been widely used as an extracellular electrical interface to record action potentials and stimulate neurons [1]. Microelectrode arrays (MEA) that have multiple micrometer scale electrodes offer high spatial resolution of electrical recording and stimulation, which are essential for the analysis of neural networks. Metal-type MEA have been successfully used to control prosthetic devices with recorded neural signals [2] or to induce plastic changes in brain circuitry by electronic stimulations [3]. Moreover, microelectrodes have been used as the electronic interface for in vitro neural tissues. Planar-type MEA is a good example that provides an experimental platform for the extracellular recording and stimulation of in vitro neural networks [4]. MEAs have been successfully used to investigate neural circuits in brain slices or dissociated neuronal cultures and have been actively developed for cell-based biosensing systems [5].

The electrical impedance of microelectrodes from electrode-electrolyte interface is an important measure for evaluating the performance of neural interfaces. In general, a high performance neural microelectrode exhibits low impedance values, which will result in low background noise for neural recordings and large charge

Correspondence: Prof. Yoonkey Nam, Dept. of Bio and Brain Engineering, KAIST, Daejeon, Korea
E-mail: ynam@kaist.ac.kr

Abbreviations: AFM, atomic force microscopy; **AC**, alternating current; **CAD**, computer-aided design; **DC**, direct current; **DI**, deionized water; **DIV**, days in vitro; **HBSS**, Hank's balanced salt solution; **ICP**, inductively coupled plasma; **IPA**, isopropyl alcohol; **MEA**, microelectrode array; **MO**, Missouri; **ms**, millisecond; **PBS**, phosphate buffered saline; **PCB**, printed circuit board; **PECVD**, plasma-enhanced chemical vapor deposition; **rms**, root mean square; **SD**, standard deviation; **Vpp**, voltage peak-to-peak

injection limits for electrical stimulations [6]. As the electrode size increases, the electrode impedance decreases and low thermal noises are obtained [4]. So, if possible, it is desired to increase the electrode size for high sensitivity in sensing neural signals. Meanwhile, the geometrical area of the electrode is desired to be small enough to address individual neurons during recording and stimulation. Thus, the trade-off between the sensitivity and selectivity is often realized by limiting the geometrical area of the electrode to the size of a single neuron and maximizing the real electrode surface area by modifying the electrode surfaces. Such surface modification has been attempted by enlarging the real surface area with platinum black [7, 8], titanium nitride [9], iridium oxide films [6, 10], carbon nanotube [11–14], and conductive polymer [15, 16]. In case of gold-based approaches, several gold nanostructures were proposed for the surface modification of neural electrodes. Aluminum templates have been widely used to fabricate gold nanostructures such as nanopillars [17] and nanorods [18]. The pillar and rod structures reduced the impedance values by increasing the surface areas. Microscale spine-shape protruded electrodes were fabricated by photolithography and electroplating to enhance the adhesion between the cell and the electrode [19]. Recently, Kim et al. [20] have reported a novel nanostructured gold miciroelectrode ("gold nanoflake"), which was fabricated by a voltage-controlled electrochemical deposition method. Despite the excellent biocompatibility and conductivity, there have been only a few reports on the fabrication methods for gold-based nanostructures dedicated for neural electrodes.

In this work, we manufactured a single-cell sized microelectrode that has novel gold grain-shaped nanostructures ("nanograin") on its surface. The fabrication was conducted through a simple electrochemical deposition method. Nanograin microelectrodes were constructed on flat gold microelectrodes and their morphological and electrical properties were characterized using electron microscopy and electrochemical techniques. The nanostructures enlarged the real surface area of an electrode, resulting in low impedance level and increased injectable electrical charges compared to flat gold microelectrodes. Finally, rat hippocampal neurons were cultured on nanograin electrodes to demonstrate the extracellular recording and stimulation performance of nanograin microelectrodes.

2 Materials and methods

2.1 MEA fabrication

Microelectrode array was fabricated by two steps: mini-MEA fabrication and printed circuit board (PCB) packaging. The mini-MEA fabrication started with MEA layout design. The layout with electrodes, pads, and connection lines were designed by a computer-aided design (CAD) tool (Autocad, Autodesk, USA) and transferred to a chrome mask. The formation of electrode arrays was followed after the mask design. An 8 inch glass wafer was rinsed by acetone, isopropyl alcohol (IPA), and deionized water (DI) and oxygen plasma was treated for 10 min. Twenty nanometer-thick titanium film and 200 nm-thick gold film were sputtered onto the wafer. The titanium layer was used to strengthen the adhesion between glass and gold. After the deposition of metal layers, the pattern of the chrome mask was transferred to the metal layers using photolithography. The metal pattern was formed through inductively coupled plasma (ICP) dry etching process with chloride and argon gas. The etched glass wafer was washed with acetone and the photoresist pattern was removed by oxygen ashing. An insulation layer was covered onto the metal pattern. A 500 nm-thick silicon nitride layer was deposited by the plasma-enhanced chemical vapor deposition (PECVD) method. The pattern of electrodes and pads was transferred onto the silicon nitride layer by photolithography. Microelectrodes and contact pads were opened by dry etching using fluoroform, argon, and oxygen gas and photoresist was removed. Finally, the wafer was cut into squares (25×25 mm^2). Aforementioned process was provided by National Nanofabrication Center (Daejeon, Korea). The second step of MEA fabrication was connecting a mini-MEA to a PCB. The PCB worked as an interface system between a mini-MEA and a commercially available amplifier. The PCB was designed by Orcad 16.3 (Cadence) and produced by Hansaem Digitec (Incheon, Korea). Two types of pads were designed on the PCB: contact pads for amplifier and wire bonding pads for a mini-MEA. The pad of the mini-MEA and the contact pad on PCB were linked by wire bonding. The wire bondings were encapsulated by epoxy (PT-4100; Supporting information, Fig. S1).

2.2 Electrochemical deposition

Gold nanograins were fabricated on the surface of gold microelectrodes by electrochemical deposition. The deposition was conducted with an aqueous solution containing 25 mM $HAuCl_4$ ($HAuCl_4 \cdot 3H_2O$, Sigma-Aldrich, MO, USA) and 20 g/L polyvinylpyrrolidone (PVP, K 30, Fluka, MO, USA). PVP was used as a surfactant that serves as a stabilizing agent. The electrochemical cell was a two-electrode system with an Ag/AgCl (3 M KCl) electrode (Nomadien, Seoul, Korea) as a reference/counter electrode and gold microelectrodes as working electrodes. Before the electrodeposition, the MEA was cleaned with acetone, IPA and DI for 5 min using ultra-sonication bath. A fixed electrochemical potential was applied through a DC power supply (E3631A, Agilent) for 10 to 60 s. After the deposition, the entire MEA chip was rinsed with acetone, IPA, and DI to remove impurities. MEA chip was blow-dried with compressed air.

2.3 Electrical characterization

Electrode-electrolyte interfacial impedance values were measured by LCR meter (E4980A, Agilent) with a large flat gold electrode (area 1.4 × 2.7 mm^2) as a reference electrode. The measurement was performed by submerging the working electrodes with 1×PBS (phosphate buffered saline, pH 7.4). The magnitude of a test signal was 100 mV_{pp} and the frequency was varied from 100 Hz to 100 kHz.

For the estimation of charge injection limits, negative–positive biphasic current pulses (amplitude: 0–60 μA, pulse width: 200 μs to 1 ms) were used with an Ag/AgCl electrode (Nomadien, Seoul, Korea) as a reference electrode. Measurements were carried out in physiological conditions using 1× PBS solution. The controlled currents were generated by a custom-built voltage-controlled current source and currents were measured by a current preamplifier (SR570, Stanford research systems) and electrode voltages were measured by instrumentation amplifier (AD622, Analog Device). NI9215 (National Instrument, USA) was used to digitize the analog signals with the sampling frequency of 25 kHz. (see Supporting information, Fig. S2 for the detailed experimental setup).

2.4 MEA surface preparation and cell culture

To culture neurons on an MEA chip, the MEA surface was coated with polydopamine ($C_8H_{11}NO_2$·HCl, 2 mg/mL in 10 mM Tris buffer, pH 8.0, Sigma-Aldrich) for 1 h [21]. After rinsing with DI, the chip was treated with air plasma (Cute, Femto Science, 30 W) for 1 min. Then, poly-D-lysine (0.1 mg/mL in 10 mM Tris buffer, pH 8.0, Sigma-Aldrich) was coated for 1 h to promote the neuronal adhesion and growth.

Hippocampi were dissected from an E-18 Sprague-Dawley rat brain by a microsurgical procedure. The dissected hippocampi were rinsed with Hank's balanced salt solution (HBSS, WelGENE Inc, Daegu, Korea) and triturated using a micropipette. The cell suspension was centrifuged for 2 min at 1000 rpm and cell pellet was extracted. The cell pellet was triturated again in Neurobasal media supplemented with B-27 (Invitrogen, CA, USA), 2 mM GlutaMAX (Gibco®, Life Technologies™), 12.5 μm L-glutamic acid (Sigma, MO, USA) and Penicillin–Streptomycin (Invitrogen, CA, USA). The cell seeding density was 800 cells/mm^2. The cell culture was stored in an incubator (5% CO_2 and 37°C) and half of media was replaced with fresh culture media without L-glutamic acid every 3 days.

2.5 Recording and stimulation

The neural signals from an MEA were recorded using an MEA 1060-BC amplifier (gain: 1100, bandwidth: 10 Hz–5 kHz, Multi Channel Systems, Reutlingen, Germany). Temperature and CO_2 concentration was maintained at 37°C and 5% CO_2 during the experiments. Amplified signals were digitized by MC Card (sampling frequency: 25 kHz, Multi Channel Systems) and processed by MC Rack program (Multi Channel Systems). The recorded data were filtered with a 200 Hz digital high-pass filter (digital filter: Butterworth, 2nd order) and extracellular action potentials were detected by setting the threshold level at six times the standard deviation of the background noise level. Electrical stimuli were applied to cultured neural networks using an STG 2004 stimulator (Multi Channel Systems, Germany). A negative-first biphasic pulse was used as a stimulus waveform. The current levels were 20–60 μA and the pulse widths were 200–1000 μs for each phase. Cultured networks that were older than 14 *days in vitro* (DIV) were used for experiments.

2.6 Immunohistochemistry and imaging

Neural cultures were fixed in 4% paraformaldehyde (Sigma, USA) for 15 min at room temperature. After rinsing the sample with PBS for several times, the cultures were permeated by 1% Triton X-100 (Sigma, USA) for 15 min at room temperature and rinsed with PBS. The cultures were immersed into the blocking solution which was 6% BSA (bovine serum albumin, Sigma, USA) for 30 min at room temperature and washed with PBS. Then, the cultures were incubated with 1.5% BSA solution mixed with primary antibodies at 37°C for 60 min. For primary antibodies, anti-β-tubulin III (anti-rabbit, 1:500, Sigma) and monoclonal anti-MAP2 (anti-mouse, 1:500, Sigma) were used. The cultures were rinsed several times by PBS and incubated with 1.5% BSA solution mixed with secondary antibodies at 37°C for 60 min. The secondary antibodies were Alexa Fluor 488 (anti-rabbit, 1:100, Invitrogen, USA) and Alexa Fluor 594 (anti-mouse, 1:100, Invitrogen). After rinsing the cultures with PBS for several times, PBS mixed with Hoechst 33342 (2.5 μg/mL, Sigma) was applied for 5 min at room temperature.

Fluorescence images were obtained by Olympus BX51M upright microscope (Olympus, Japan) with 20× water immersion objective lens. Bright-field images were taken by Olympus IX-71 inverted microscope (Olympus, Japan) under phase-contrast mode.

3 Results

3.1 Electrodeposition of gold nanograins

Gold nanograins were electrochemically deposited onto a flat thin-film gold microelectrode (thickness: 20 nm). The morphology of gold nanograins was mostly dependent upon the electrodeposition time. Figure 1A and B show the time course of the formation of gold nanograin structures on a flat gold microelectrode (diameter: 10 μm)

encircled with silicon nitride insulation layer (thickness: 500 nm). When a reduction voltage of –0.3 V was applied for 10 s, there was a nucleation of gold seeds whose sizes were about 20–70 nm. After 30 s, round shape grains that had a diameter of 100 nm were formed on the electrode surface and they were also formed outside the electrode opening area (Fig. 1A). After 60 s of deposition, it was noticeable that there were micrometer scale smooth ellipsoidal structures ("micropetals") with the size of 1–5 μm at the circumference of the microelectrode. At the center of the electrode surface, round-shaped grains were enlarged to 500 nm in diameter. Overall, the final electrode structure was a "sunflower" shape (Fig. 1B). Investigating the sub-micrometer scale, micropetals, and round grains were composed of many nanograins (Fig. 1C). These nanograins were again composed of sub-grains in the size of a few tens of nanometers. The gold nanograins increased the real surface area of microelectrodes. When the surface roughness was inspected with atomic force microscopy (AFM), we confirmed that the nanograins increased the surface roughness (Supporting information, Fig. S3). The mean surface roughness of a gold nanograin electrode and a flat gold electrode were 380 and 8.61 nm, respectively.

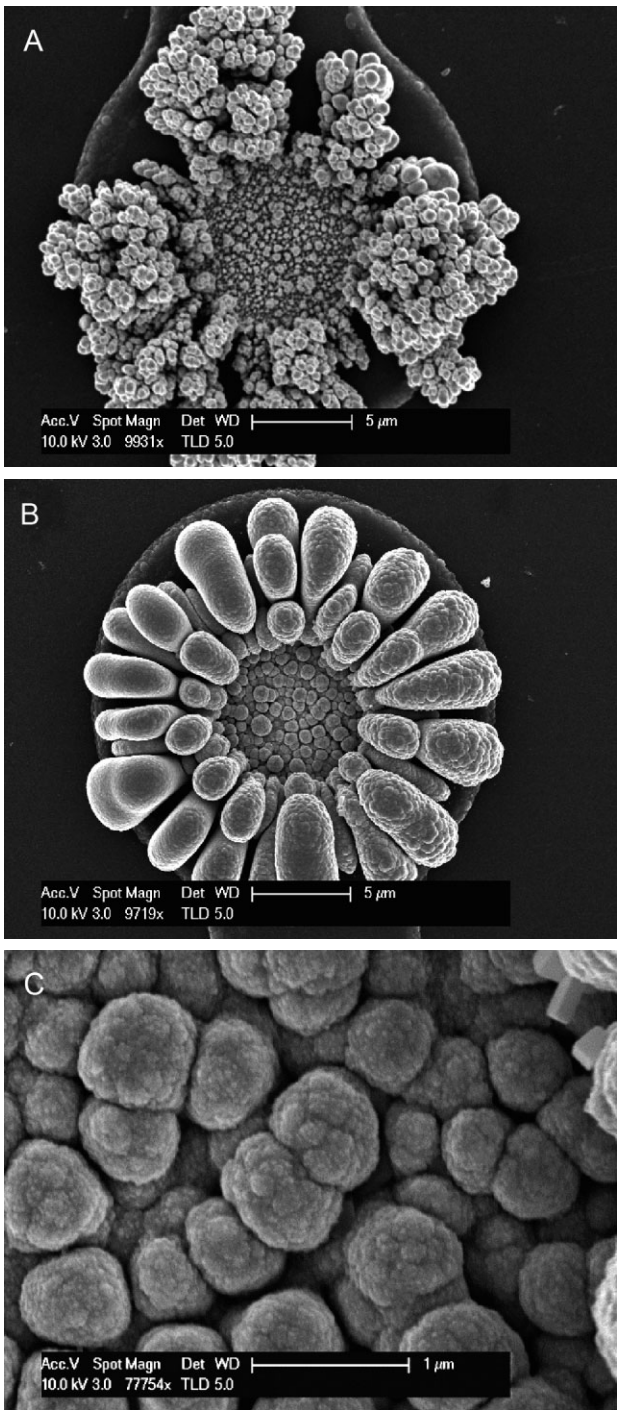

Figure 1. Representative SEM images of gold nanograin structures. The morphologies of nanograin microeletrodes after (**A**) 30-s electrochemical deposition and (**B**) 60-s deposition. Nanometer scale grains and micropetals were formed at 60 s. (**C**) The enlarged image of nanograins in (**B**). Electrode size: 10 μm diameter. Deposition condition: $V = -0.3$ V. Each experiment was repeated at least 7 times.

The electrochemical reduction potential and the diameter of an electrode did not have a significant influence on the formation of nanograin structures. When we applied voltages between –0.25 and –0.4 V for 60 s, the micropetal and nanograin structures were similar in their shapes and sizes (Supporting information, Fig. S4). The nanograins and micropetals were consistently formed on microelectrodes with various sizes under the same deposition condition. We confirmed that the different size of electrodes (diameter: 10, 20, 30, 40, and 50 μm) had similar nanograin structures (Supporting information, Fig. S5).

3.2 AC impedance characteristics of microelectrodes

Electrode-electrolyte interface was characterized by measuring the AC impedance values. The electrode impedance level is desired to be less than hundreds of kilo-ohms for low thermal noise level and high sensitivity to neural signals [4]. According to the previous section, nanograins increased the electrode real surface area, which would increase the double-layer capacitance and lower the AC impedances. Figure 2A shows the change of AC impedance magnitude at 1 kHz for 10 μm-diameter electrodes. We traced seven different electrodes and measured the impedance values at 10, 30, and 60 s after the deposition. After 10-s, impedance was decreased by 57% from the original value, but it was still large (5.0 ± 0.6 MΩ, mean ± SD, $N = 7$). There was only a small nucleation of gold seeds on the electrode surface (data not shown), thus the impedance reduction was not large enough to reach a hundred kilo-ohm range. After 30-s deposition, impedance level reached to 126 ± 37 kΩ (mean ± SD, $N = 7$) and the large reduction was mainly due to nanograins on surfaces and circumferences of the

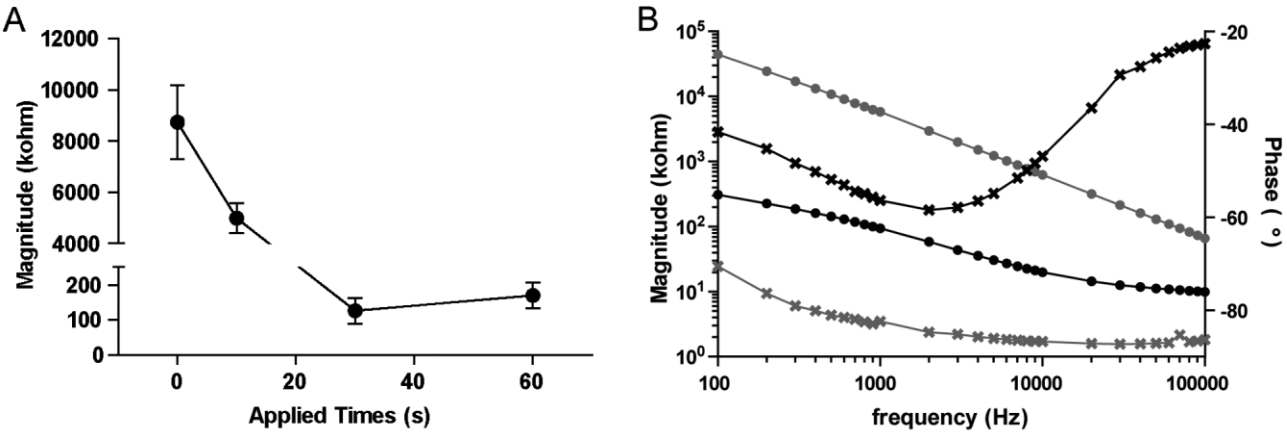

Figure 2. AC Impedance characterization of gold nanograin electrodes. (**A**) AC impedance values (magnitudes at 1 kHz) versus electrodeposition time. Mean ± SD ($N = 7$). (**B**) AC impedance values versus frequency. Circles are magnitude and crosshairs are phase angles. Gray: flat gold electrode, black: nanograin electrode. Electrode size: 10 μm diameter. Deposition condition: $V = -0.3$ V.

electrodes. It also implied that these nanograins were electrically connected with each other (Fig. 1A). After 60-s deposition, the average impedance value was 170 ± 37 kΩ (mean ± SD, $N = 7$). The slight increase in impedance values after 60-s deposition was due to the reduction of real surface area, which can be inferred from the increase in the size of nanograins and the formation of micropetal structures with smoother looking surfaces (see Fig. 1A and B). Judging from the original high impedance value (8.7 ± 1.4 MΩ, $N = 7$), the final impedance value in the range of 100–200 kΩ was a substantial enhancement, which would reduce the thermal noise level for recording weak neural signals. Table 1 shows the impedance values of nanograin microelectrodes formed on microelectrodes with different sizes. When we compared the geometrical size and final impedance values, microelectrodes with larger geometrical area had smaller impedance values after the deposition. Among the tested microelectrodes, 26 kΩ was the minimum impedance value obtained from the largest microelectrode whose diameter was 50 μm. In contrast to the absolute impedance values, the reduction ratio was higher for smaller microelectrodes. The reduction ratios were 69.4 for 10 μm-diameter electrode and 55.2 for 50 μm-diameter electrode, which indicated that the proposed modification scheme will be efficient for small-sized microelectrodes. Finally, we compared the impedance values for the nanograin microelectrodes (diameter: 10 μm) fabricated with different reduction voltage (–0.25–0.4 V), and they were 165 ± 47 kΩ, 246 ± 35 kΩ, and 301 ± 20 kΩ (mean ± SD, $N = 7$) for –0.25, –0.35, and –0.4 V, respectively.

Figure 2B shows AC impedance spectrum measured in the frequency ranging from 100 Hz to 100 kHz for 10 μm-diameter electrodes. In case of a flat gold electrode, the magnitude decreased with frequency and the phase was relatively constant near –86.5°. This implied that the electrode interface impedance was mainly dominated by constant phase element or pseudo-capacitance [6]. After modifying the flat gold microelectrode with nanograins, impedance magnitudes decreased by nearly two orders of magnitudes in all frequencies and the phase changed from –56.4° at 1 kHz to nearly –20° at 100 kHz. The decrease of magnitude and increase of phase indicated that the double-layer capacitance was increased and the electrode–electrolyte interface became more resistive.

Table 1. Impedance values before and after nanograin formation ($f = 1$ kHz)[a)]

Electrode diameter (μm)	Flat electrode		Nanograin electrode		Impedance reduction ratio (Ω/Ω)
	Magnitude (MΩ)	Phase (°)	Magnitude (kΩ)	Phase (°)	
10	8.74 ± 1.44	–86.5 ± 0.77	126.0 ± 36.8	–56.0 ± 3.16	69.4
20	5.03 ± 0.25	–86.9 ± 0.62	58.4 ± 23.2	–63.6 ± 10.1	86.1
30	3.51 ± 0.44	–86.4 ± 0.81	61.1 ± 13.7	–72.3 ± 13.3	57.5
40	1.92 ± 0.15	–85.3 ± 0.44	33.0 ± 10.2	–68.4 ± 9.92	58.2
50	1.48 ± 0.14	–85.7 ± 0.20	26.8 ± 5.9	–66.0 ± 7.75	55.2

[a)]Deposition condition: –0.3 V, 60 s. Data show mean ± SD, $n = 5$.

3.3 Estimation of charge injection limits for microstimulations

We estimated the charge injection limit of gold nanograin electrodes using biphasic current pulses. Negative-positive ("cathodic first") biphasic current pulses were applied to a nanograin electrode (geometrical area: 78.5 μm^2) and electrical voltages were measured between the electrode and reference electrode (Ag/AgCl). The exact electrode potential was calculated by subtracting the ohmic voltage drop owing to the electrolyte resistance from the measured voltage (Supporting information, Fig. S2). The injection charge was varied by changing either current amplitudes or pulse widths and the final electrode voltage at the end of negative current pulse was used to determine the charge injection limit.

Figure 3A shows the electrode voltage of nanograin electrodes when current amplitudes were applied from 5 to 60 μA with the fixed pulse width of 200 μs. When a negative current pulse was applied, the electrode voltage decreased as negative charges accumulated at the electrode-electrolyte interface ("double-layer"). When the current was reversed to a positive value, the electrode potential increased as the accumulated negative charges were removed. When the current pulses were turned off, the electrode voltage returned to its original value by slow discharging. When the amount of injection charge increased, the electrode voltage reached to a limiting value indicating the occurrence of faradaic reactions on the electrode surfaces. At this point, the further charge injection will lead to an electrochemical reaction such as electrolysis which can alter pH or generate gas bubbling near the electrode. Figure 3B shows electrode voltages when the injection charges were increased by increasing the pulse width (PW: 100–1000 μs) at a fixed current of 20 μA. In both cases, charge injections were limited by the faradaic reactions indicated by the flat region. We measured the cathodic electrode voltage with the negative injection charges ranging from 1 to 20 nC (Fig. 3C). In case of amplitude-based charge modulation, maximum charge was limited to 8 nC and the estimated charge injection limit was calculated to be 10.2 mC/cm^2 (geometrical area: 78.5 μm^2). In case of pulse width modulation, the maximum value was 12 nC. These charge injection limits were comparable to the reported values reported from in vivo or in vitro tests with similar sizes of microelectrodes [22, 23]. In case of an unmodified flat gold microelectrode (geometrical area: 78.5 μm^2), the maximum injectable charge was estimated to be 0.8 nC (1.02 mC/cm^2). It clearly indicated that the gold nanograins improved the charge injection limits for microstimulations. We also tested the charge injection limit for different sizes of microelectrodes. The charge injection limits were 2.87 (geometrical area: 707 μm^2), 3.18 (geometrical area: 1256 μm^2), 2.12 (geometrical area: 2826 μm^2), 1.59 (geometrical area: 5024 μm^2), and 1.27 mC/cm^2 (geometrical area: 7850 μm^2).

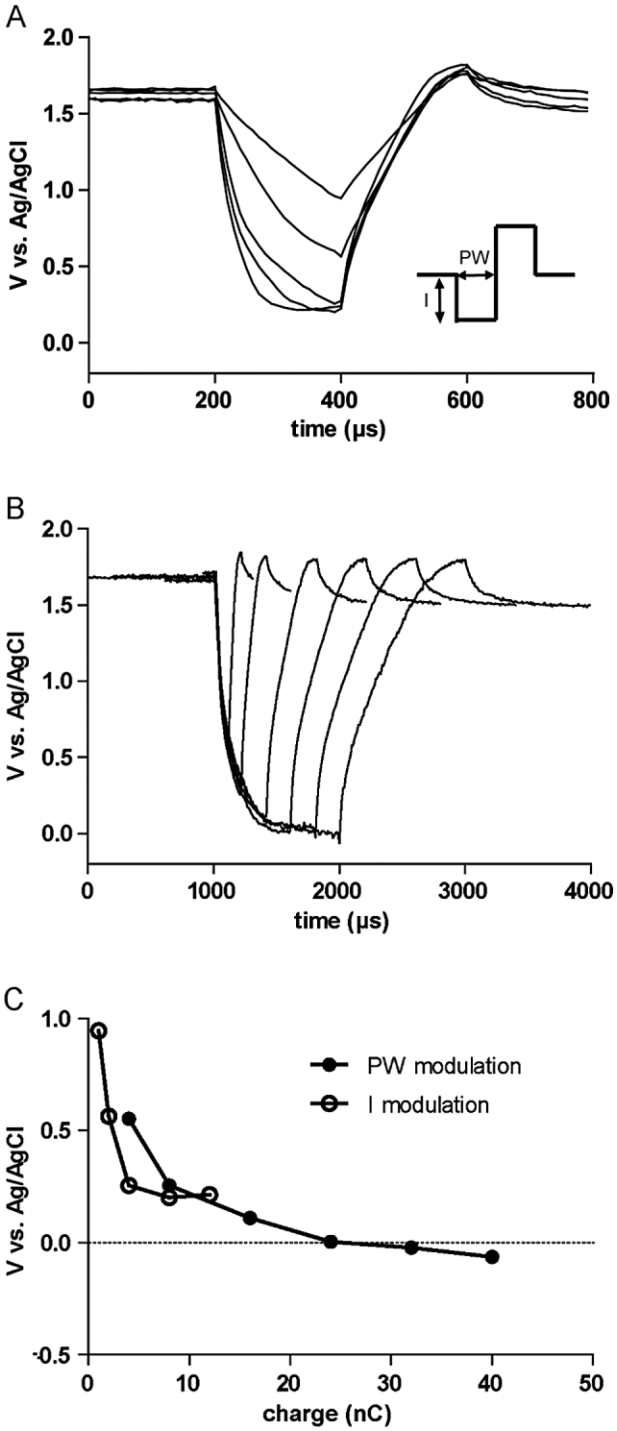

Figure 3. Electrode voltage measurement for biphasic current pulses. Injection charges at negative phase were controlled by varying (**A**) current amplitudes or (**B**) pulse width (PW). (**A**) Current amplitudes: 5, 10, 20, 40, and 60 μA, pulse width: 200 μs. (**B**) Current amplitude: 20 μA, pulse width: 200, 400, 800, 1200, 1600, and 2000 μs. (**C**) Injected negative charge versus minimum cathodic voltage. Electrode size: 10 μm. Each trace is an average of 10 repeats.

Biotechnol. J. 2013, 8, 206–214

3.4 Mechanical durability of nanograin microelectrodes

The mechanical stability of gold nanograin electrodes was tested by measuring impedance before and after various tests. In order to test the durability for cell culture preparation, we performed an intensive surface rinsing with acetone, IPA, and DI water. The magnitude increased from 113 ± 19 kΩ (mean ± SD, N = 30) to 197 ± 35 kΩ (mean ± SD, N = 30), which was acceptable for neural recordings. Then, a piece of adhesive tape (MMM600341296, 3M, St. Paul, MN, USA) was attached onto the surface of MEA and removed. After the adhesive-tape peel test, the magnitude increased to 392 ± 163 kΩ (mean ± SD, N = 30), which indicated that the nanostructures were broken by mechanical impulse. These tests showed that the gold nanograin electrodes were durable for moderate conditions for neural recording and stimulation.

3.5 Recording and stimulation of hippocampal neural networks in vitro

We cultured dissociated rat hippocampal neurons on a 60-channel MEA. Figure 4A is a phase-contrast image of a cultured neural network on an MEA at 14 DIV and Fig. 4B is fluorescently labeled cytoskeletons (green, β-tubulin III) of matured cultured neurons shown in Fig. 4A. There were rich neurite outgrowth and networking among neurons on MEAs and somata (cell bodies, the arrowheads in Fig. 4B) were growing near the nanograin electrodes (the dashed circle in Fig. 4B). Cultured neurons remained healthy for a month, which confirmed the biocompatibility of modified gold nanograin electrodes.

Spontaneous electrical signals from hippocampal neuronal cultures were readily recordable at 14 DIV. In the inset of Fig. 4A, a typical electrical signal is shown which was originated from one of two neurons (arrowheads in

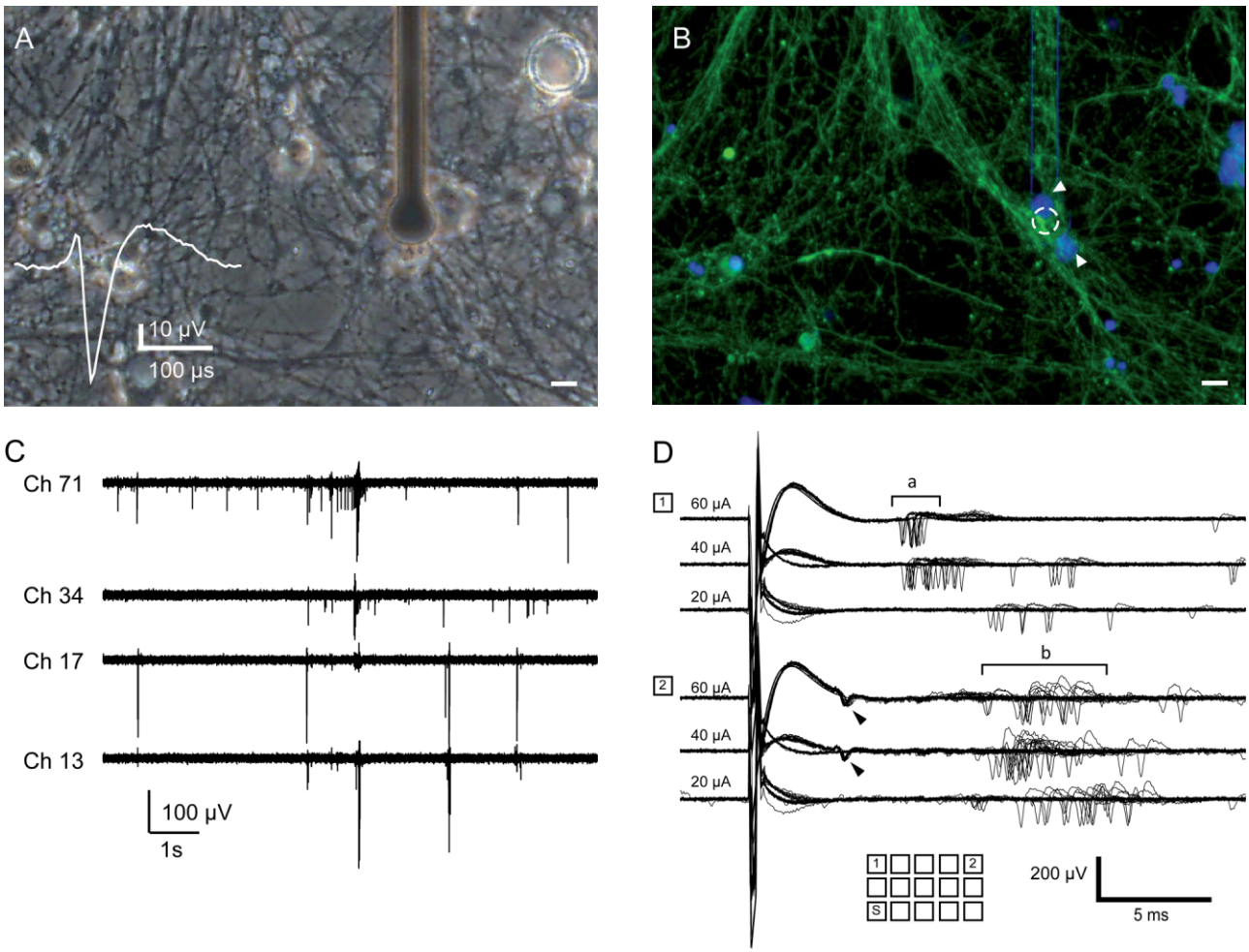

Figure 4. Neuronal culture tests using MEAs. (**A**) Phase-contrast optical image of live neural networks cultured on an MEA. The inset shows a representative extracellular action potential detected from a nanograin microelectrode. (**B**) Fluorescence image of immunolabelled neurons in (**A**) (green: β-tubulin III, blue: nuclei). The white circle indicates a nanograin electrode. The scale bars in (**A**) and (**B**) are 10 μm. (**C**) Multichannel recordings of spontaneous neural activity from matured neuronal networks at 14 DIV. (**D**) Stimulation and recordings of neuronal networks in vitro. Inset: stimulating electrode (S), recording electrodes (1, 2). Electrode spacing was 200 μm. Each row is overlapped responses of 30 consecutive trials with identical current pulses.

Fig. 4B) and it was recorded by the nanograin electrode near these neurons. Figure 4C shows neural signals from a cultured neural network, which were recorded simultaneously by several channels of an MEA. The recorded extracellular action potentials ("spikes") were measured to be in the range of 18.6–315 μV (zero-to-peak) and the background noise level was 2.89 μV_{rms}. As the spikes were detected by setting the threshold level at 6 times the standard deviation of the noise, very small neural signals can be detected with high confidence level. The signal-to-noise ratio, which was calculated by dividing the zero-to-peak values of signal and noise, was estimated to be 1.3–21.8.

Figure 4D shows a series of electrical stimulation and recording from cultured neuronal networks at 14 DIV. A charge-balanced biphasic current pulses (20, 40, and 60 μA; pulse width: 200 μs) were applied to a single electrode ("S") with the rate of 0.5 pulses/s and the following responses were recorded from the distant nanograin electrodes ("1" and "2" in Fig. 4D). Various neural responses could be evoked from the nanograin microelectrodes. Phase-locked early neural responses (the arrowheads in Fig. 4D) were recorded when the stimulus level was increased from 20 to 40 μA. The onset time of the response was precisely fixed at 4.2 ms and it occurred with a high probability. The precise responses can also be observed in another electrode when the stimulus level was increased from 40 to 60 μA. The onset spikes were more concentrated on a 1-ms time window ("a" in Fig. 4D) and the probability of spike occurrence also increased. There were some delayed responses appearing around 16 ms ("b" in Fig. 4D). Although it was estimated that a negative current pulse of 60 μA/200 μs can accompany faradaic reactions on the electrode surfaces (Fig. 3A), a low pulse rate did not seem to induce serious damage to nearby neurons immediately as they were producing reliable and reproducible responses for repeated stimuli. The quality of measured neural signals from cultured neurons were comparable to other types of microelectrodes, which shows that nanograin electrodes have a good potential to be adopted by neurophysiological experiments [24].

4 Discussion

We were able to obtain a single-cell sized novel gold microelectrode for neural interfaces using a simple electrochemical deposition method. The fabrication technique was effective in reducing the impedance and increasing the stimulation capability of a single-cell sized microelectrodes. There have been only a few reports on gold-based nanostructured neural electrodes even though gold has excellent biocompatibility and conductivity. Gold nanopillars were fabricated using an aluminum oxide template [17]. Nanoporous gold electrodes have been reported, which used gold-silver alloy annealing method [25]. Our gold nanograin electrodes were fabricated with a relatively simple electrochemical deposition method using two-electrode system. In our previous study, a similar set-up was used to fabricated flake-shape nanostructures using a different type of reference electrode (a graphite sheet) and longer deposition time (60 min) [20]. In our current setup, we were able to replicate the nanoflake structures using a large flat gold reference electrode (area: 1.4 × 2.7 mm^2) under the same deposition condition (–0.3 V, 60 min; Supporting information, Fig. S6). Interestingly, we obtained gold nanograin electrodes by simply switching the reference electrode from a polarizable gold film electrode to non-polarizable Ag/AgCl electrode and shortening the deposition time to 60 s. The selection of a different reference electrode would have altered the standard half-cell potential for the electrochemical cell and the corresponding kinetics of the redox reactions. Even though the same potential was applied to the electrochemical cell, different kinetics of gold ions may have resulted in different types of nanostructures.

The electrical properties were also improved by our nanograin structures. The gold nanopillars had the noise level of 6.6 μV_{rms} for electrodes 10 μm in diameter and nanoporous gold showed 25-fold reduction of electrical impedance for electrodes 30 μm in diameter [17, 25]. Gold nanoflake electrode had 57.8-fold of impedance reduction with electrodes 10 μm in diameter [20]. Our gold nanograin electrodes had 69-fold reduction effect in electrical impedances and RMS noise level as small as 2.89 μV for electrodes 10 μm in diameter. This noise level was comparable to other types of gold-based nanostructured electrodes. The main reason for the improvement of properties was the formation of nanograins and micropetals, which increased the real electrode surface area of a microelectrode. In case of charge injection limit, we obtained 10.2 mC/cm^2 for microelectrode 10 μm in diameter (geometrical area: 78.5 μm^2), which was comparable to the value reported from Pt–Ir microelectrodes (geometrical area: 100 μm^2) for intracorical stimulations (10 mC/cm^2) [26]. For larger microelectrodes (707, 1256, 2826, 5024, and 7850 μm^2), the estimated values (2.83, 3.18, 2.12, 1.59, and 1.27 mC/cm^2, respectively) were comparable to carbon nanotube coated electrodes (0.8 mC/cm^2, geometrical 92 300 μm^2 [11]) and nanoporous platinum electrode (3 mC/cm^2, geometrical area: 1600 μm^2 [7]). Finally, neural activities were readily recorded from nanograin electrodes and electrical stimulations were efficiently transferred to neural networks producing action potential response. The absolute magnitude of action potentials were not very high when compare to other gold electrodes [17, 20, 27]. However, the electrode showed very low RMS noise level so that small signals can be readily detected. This novel nanostructured neural electrode will be applied to develop highly sensitive cell-based biosensors or clinical neural prosthetic devices, such as deep brain stimulation.

This research was supported by the National Research Foundation of Korea (KRF-2008-313-D00614, 2012007327), the Korea Ministry of Education, Science and Technology (MEST) through the Brain Research Center of the 21st Century Frontier Research Program (22-2009-00-002-00) and the Industrial Source Technology Development Program (10033657) of the Ministry of Knowledge Economy (MKE).

The authors declare no conflict of interest.

5 References

[1] Normann, R., Technology insight: Future neuroprosthetic therapies for disorders of the nervous system. *Nat. Clin. Pract. Neurol.* 2007, *3*, 444–452.
[2] Hochberg, L. R., Serruya, M. D., Friehs, G. M., Mukand, J. A et al., Neuronal ensemble control of prosthetic devices by a human with tetraplegia. *Nature* 2006, *442*, 164–171.
[3] Jackson, A., Mavoori, J., Fetz, E. E., Long-term motor cortex plasticity induced by an electronic neural implant. *Nature* 2006, *444*, 56–60.
[4] Nam, Y., Wheeler, B. C., In vitro microelectrode array technology and neural recordings. *Crit. Rev. Biomed. Eng.* 2011, *39*, 45–61.
[5] Stett, A., Egert, U., Guenther, E., Hofmann, F. et al., Biological application of microelectrode arrays in drug discovery and basic research. *Anal. Bioanal. Chem.* 2003, *377*, 486–495.
[6] Cogan, S. F., Neural stimulation and recording electrodes. *Ann. Rev. Biomed. Eng.* 2008, *10*, 275–309.
[7] Park, S., Song, Y. J., Boo, H., Chung, T. D., Nanoporous Pt microelectrode for neural stimulation and recording: In vitro characterization. *J. Phys. Chem. C* 2010, *114*, 8721–8726.
[8] Sekirnjak, C., Hottowy, P., Sher, A., Dabrowski, W. et al., High-resolution electrical stimulation of primate retina for epiretinal implant design. *J. Neurosci.* 2008, *28*, 4446–4456.
[9] Weiland, J. D., Anderson, D. J., Humayun, M. S., In vitro electrical properties for iridium oxide versus titanium nitride stimulating electrodes. *IEEE Trans. Bio-med. Eng.* 2002, *49*, 1574–1579.
[10] Negi, S., Bhandari, R., Rieth, L., Van Wagenen, R. et al., Neural electrode degradation from continuous electrical stimulation: Comparison of sputtered and activated iridium oxide. *J. Neurosci. Methods* 2010, *186*, 8–17.
[11] Ansaldo, A., Castagnola, E., Maggiolini, E., Fadiga, L. et al., Superior electrochemical performance of carbon nanotubes directly grown on sharp microelectrodes. *ACS Nano* 2011, *5*, 2206–2214.
[12] Fung, A. O., Tsiokos, C., Paydar, O., Chen, L. H. et al., Electrochemical properties and myocyte interaction of carbon nanotube microelectrodes. *Nano Lett.* 2010, *10*, 4321–4327.
[13] Gabay, T., Ben-david, M., Kalifa, I., Sorkin, R. et al., Electro-chemical and biological properties of carbon nanotube based multi-electrode arrays. *Nanotechnology* 2007, *18*, 035201.
[14] Keefer, E. W., Botterman, B. R., Romero, M. I., Rossi, A. F. et al., Carbon nanotube coating improves neuronal recordings. *Nat. Nanotechnol.* 2008, *3*, 434–439.
[15] Cui, X., Lee, V. A, Raphael, Y., Wiler, J. A et al., Surface modification of neural recording electrodes with conducting polymer/biomolecule blends. *J. Biomed. Mater. Res.* 2001, *56*, 261–272.
[16] Venkatraman, S., Hendricks, J., King, Z. A, Sereno, A. J. et al., In vitro and in vivo evaluation of PEDOT microelectrodes for neural stimulation and recording. *IEEE Trans. Neural Syst. Rehabil. Eng.* 2011, *19*, 307–316.
[17] Brüggemann, D., Wolfrum, B., Maybeck, V., Y, M. et al., Nanostructured gold microelectrodes for extracellular recording from electrogenic cells. *Nanotechnology* 2011, *22*, 265104.
[18] Zhou, H., Li, G., Sun, X., Zhu, Z. et al., Integration of Au nanorods with flexible thin-film microelectrode arrays for improved neural interfaces. *J. Microelectromech. Syst.* 2009, *18*, 88–96.
[19] Hai, A., Shappir, J., Spira, M. E., In-cell recordings by extracellular microelectrodes. *Nat. Methods* 2010, *7*, 200–202.
[20] Kim, J.-H., Kang, G., Nam, Y., Choi, Y.-K., Surface-modified microelectrode array with flake nanostructure for neural recording and stimulation. *Nanotechnology* 2010, *21*, 85303.
[21] Kang, K., Choi, I. S., Nam, Y., A biofunctionalization scheme for neural interfaces using polydopamine polymer. *Biomaterials* 2011, *32*, 6374–6380.
[22] Torab, K., Davis, T. S., Warren, D. J., House, P. A et al., Multiple factors may influence the performance of a visual prosthesis based on intracortical microstimulation: Nonhuman primate behavioural experimentation. *J. Neural Eng.* 2011, *8*, 035001.
[23] Sekirnjak, C., Hottowy, P., Sher, A., Dabrowski, W. et al., Electrical stimulation of mammalian retinal ganglion cells with multielectrode arrays. *J. Neurophysiol.* 2006, *95*, 3311–3327.
[24] Marom, S., Shahaf, G., Development, learning and memory in large random networks of cortical neurons: Lessons beyond anatomy. *Q. Rev. Biophys.* 2002, *35*, 63–87.
[25] Seker, E., Berdichevsky, Y., Begley, M. R., Reed, M. L. et al., The fabrication of low-impedance nanoporous gold multiple-electrode arrays for neural electrophysiology studies. *Nanotechnology* 2010, *21*, 125504.
[26] Schmidt, E. M., McIntosh, J. S., Microstimulation of precentral cortex with chronically implanted microelectrodes. *Exp. Neurol.* 1979, *63*, 485–503.
[27] Fendyur, A., Mazurski, N., Shappir, J., Spira, M. E., Formation of essential ultrastructural interface between cultured hippocampal cells and gold mushroom-shaped MEA- Toward "IN-CELL" recordings from vertebrate neurons. *Front. Neuroeng.* 2011, *4*, 1–14.